

Scattering variability detected from the circumsource medium of FRB 20190520B

Stella Koch Ocker,¹* James M. Cordes,¹ Shami Chatterjee,¹ Di Li,^{2,3} Chen-Hui Niu,² James W. McKee,⁴ Casey J. Law,^{5,6} and Reshma Anna-Thomas⁷

¹*Department of Astronomy and Cornell Center for Astrophysics and Planetary Science, Cornell University, Ithaca, NY 14850, USA*

²*National Astronomical Observatories, Chinese Academy of Sciences, Beijing 100101, China*

³*Research Center for Intelligent Computing Platforms, Zhejiang Laboratory, Hangzhou 311100, China*

⁴*Canadian Institute for Theoretical Astrophysics, University of Toronto, 60 Saint George Street, Toronto, ON M5S 3H8, Canada*

⁵*Cahill Center for Astronomy and Astrophysics, MC 249-17 California Institute of Technology, Pasadena, CA 91125, USA*

⁶*Owens Valley Radio Observatory, California Institute of Technology, 100 Leighton Lane, Big Pine, CA, 93513, USA*

⁷*Department of Physics and Astronomy and the Center for Gravitational Waves and Cosmology, West Virginia University, Morgantown, WV 26506, USA*

Accepted XXX. Received YYY; in original form ZZZ

ABSTRACT

Fast radio bursts (FRBs) are millisecond-timescale radio transients, the origins of which are predominantly extragalactic and likely involve highly magnetized compact objects. FRBs undergo multipath propagation, or scattering, from electron density fluctuations on sub-parsec scales in ionized gas along the line-of-sight. Scattering observations have located plasma structures within FRB host galaxies, probed Galactic and extragalactic turbulence, and constrained FRB redshifts. Scattering also inhibits FRB detection and biases the observed FRB population. We report the detection of scattering times from the repeating FRB 20190520B that vary by up to a factor of two or more on minutes to days-long timescales. In one notable case, the scattering time varied from 7.9 ± 0.4 ms to less than 3.1 ms (95% confidence) over 2.9 minutes at 1.45 GHz. The scattering times appear to be uncorrelated between bursts or with dispersion and rotation measure variations. Scattering variations are attributable to dynamic, inhomogeneous plasma in the circumsource medium, and analogous variations have been observed from the Crab pulsar. Under such circumstances, the frequency dependence of scattering can deviate from the typical power-law used to measure scattering. Similar variations may therefore be detectable from other FRBs, even those with inconspicuous scattering, providing a unique probe of small-scale processes within FRB environments.

Key words: transients: fast radio bursts – stars:neutron – stars: magnetars – scattering – plasmas

1 INTRODUCTION

FRB 20190520B is only the second fast radio burst (FRB) localized to a dwarf galaxy and associated with a compact persistent radio source (PRS), presumably from a synchrotron nebula surrounding the source (Niu et al. 2022). Its total line-of-sight (LOS) integrated electron density (n_e), or dispersion measure $DM = \int n_e dl / (1+z) = 1205 \pm 4$ pc cm⁻³, is dominated by the host galaxy at redshift $z_h = 0.241$, which contributes $DM_h = 903^{+72}_{-111}$ pc cm⁻³ (observer frame), at least three times the DM typically assumed for the host galaxies of non-localized FRBs (Niu et al. 2022; Ocker et al. 2022). Like some other repeating FRBs, FRB 20190520B shows extreme variations in rotation measure (RM), which are attributed to path-integrated magnetic field changes within its local environment (Feng et al. 2022; Anna-Thomas et al. 2022; Dai et al. 2022).

FRB 20190520B also shows evidence of significant scattering, observed as both pulse broadening with a corresponding temporal delay τ (aka the scattering time), and scintillation with a corresponding frequency bandwidth $\Delta\nu_d$. In Ocker et al. (2022), hereafter O22,

we measured a mean scattering time $\bar{\tau}(1.41 \text{ GHz}) = 10.9 \pm 1.5$ ms (9.5 ± 1.3 ms at 1.45 GHz) and a mean scintillation bandwidth $\Delta\bar{\nu}_d(1.41 \text{ GHz}) = 0.21 \pm 0.01$ MHz (0.23 ± 0.01 MHz at 1.45 GHz) for this source. Attributing $\bar{\tau}$ to the host galaxy and $\Delta\bar{\nu}_d$ to the Milky Way constrained the mean scattering from the host galaxy to within 100 pc of the source.

In this work we examine individual bursts from FRB 20190520B to characterize scattering variations near the FRB source. Unlike Galactic pulsar scattering, which even for the Crab pulsar varies slowly (longer than days to weeks; McKee et al. 2018), we find that the scattering time can vary significantly between bursts, indicating the presence of plasma inhomogeneities likely on sub-astronomical unit (au) scales within the circumsource medium (CSM). Section 2 describes the methods used to analyze burst spectra and constrain scattering. Results are presented in Section 3 and implications for the CSM and other FRB sources are discussed in Section 4.

2 METHODS

FRB 20190520B was initially detected in archival data from the Comensal Radio Astronomy FAST Survey (CRAFTS; Li et al. 2018;

* E-mail: sko36@cornell.edu

Nan et al. 2011). The burst sample considered in this paper is drawn from tracking observations of the FRB conducted at FAST between April and September 2020, which yielded 75 burst detections across 12 observing epochs in the 1.05 – 1.45 GHz frequency band. These observations were discussed in Niu et al. (2022), and correspond to bursts P5 - P79 in the supplementary information of that paper (for reference, bursts A-D in Figures 1-2 correspond to bursts P28, P34, P66, and P67). The same set of bursts was discussed in O22.

Bursts from FRB 20190520B show a range of morphologies, from burst intensities that are symmetric in time, to spectral islands that drift downward in frequency-time space (the “sad-trombone”), and frequency-dependent temporal widths and intensity modulations that are attributable to scattering (Niu et al. 2022; Ocker et al. 2022). We have taken a number of steps throughout the analysis to mitigate confusion of intrinsic structure with scattering asymmetries, including the exclusion of bursts with multiple identifiable components and frequency-time drift from the analysis; the assessment of scattering models in multiple frequency subbands; and the statistical evaluation of burst asymmetries used in the skewness method described below.

2.1 Initial Data Processing

The data were initially recorded in filterbank format with a frequency resolution of 0.122 MHz and a sampling time of 49.5 μ s. The data were subsequently smoothed to a temporal resolution of 1.57 ms using a 1D boxcar filter, except for burst D, for which a temporal resolution of 0.59 ms was used to obtain adequate sampling across the burst.

Two de-dispersion methods were explored, one that maximizes burst substructure (Hessels et al. 2019) and one that maximizes burst peak S/N (Cordes & McLaughlin 2003). While structure-optimization is generally favored for bursts that have multiple components and non-dispersive frequency-time drift, the scattering times of such bursts are highly ambiguous even after de-dispersion. We therefore removed bursts with non-dispersive frequency-time drift and/or multiple identifiable components (peak S/N $\gtrsim 5$ when averaged across the entire 400 MHz band) and did not consider these bursts in subsequent analysis. For the remaining single-component bursts, we compared the structure-optimized DMs determined in Niu et al. (2022) and S/N-maximized DMs, which were determined by calculating S/N for a range of trial DMs at 0.1 pc cm⁻³ resolution. The peak and width of the resulting ambiguity function were used to determine the best-fit DM and error. There was minimal difference between the structure-optimized and S/N-maximized DMs for most of the single-component bursts in the sample. However, in some cases structure optimization misestimated the DMs of single-component bursts by failing to align the leading edge of intensity across all frequencies, which can result in an overestimated scattering time. We therefore use the S/N-maximized DMs in subsequent analysis. All dynamic spectra were individually examined to affirm that the leading edge of intensity was aligned across the burst bandwidth, before proceeding with the scattering analysis.

In most cases, burst intensity is concentrated above 1.3 GHz. We define the burst bandwidth as the range of frequencies for which averaging over a 300 ms window around the burst yields a S/N $\gtrsim 2$, and the central frequency as the mid-frequency of the burst bandwidth. The average central frequency of the burst sample is 1.35 GHz. Data from 1.16-1.29 GHz were masked for most bursts due to radio frequency interference (RFI).

2.2 Empirical Burst Widths

We measure the total, empirical width of each burst using the ACF of the burst intensity averaged over the burst’s entire spectral bandwidth, $\langle I(t)I(t + \delta t) \rangle$. The ACF error at a lag k is $\sqrt{(1/n) \times (1 + 2 \sum_{m=1}^{k-1} r_m^2)}$, where n is the length of the time series and r_m is the autocorrelation at lag m . The burst full-width-at-half-maximum (FWHM) is estimated using the half-width-at-half-maximum (HWHM) of the ACF, $\text{FWHM} = \sqrt{2} \times \text{HWHM}(\text{ACF})$ (calculated after removal of the noise spike at zero lag). For a Gaussian burst, this is equivalent to the FWHM that would be derived directly from the pulse shape. In general, $\text{FWHM} \approx \sqrt{W_i^2 + W_{\text{PBF}}^2}$, where W_i is the intrinsic burst width and W_{PBF} is the width of the PBF.

2.3 Burst Scattering Times

A canonical, robust scattering measurement generally requires that the burst intensity be asymmetric in time, with an extended scattering tail that increases at lower observing frequencies. Accurate identification of scattering thus requires an assessment not only of the pulse profile in time, but also the evolution of that profile over frequency, which in turn requires precise de-dispersion. For fitting purposes, the burst profile (intensity vs. time) is assumed to consist of a Gaussian pulse convolved with a one-sided exponential pulse broadening function (PBF), with a $1/e$ delay τ that scales with observing frequency ν as $\tau \propto \nu^{-4}$. The Gaussian pulse is assumed constant in frequency ν , while the scattering time τ , the $1/e$ time of the PBF, evolves as $\tau \propto \nu^{-4}$. Each burst was divided into multiple frequency subbands before averaging over frequency to obtain the temporal burst profile as a function of frequency. The scattering time and Gaussian width were then fit by minimizing the χ^2 statistic, and the burst amplitude was left as a free parameter that varied between subbands. While PBFs discerned from pulsar observations can be non-exponential and intrinsic widths can vary with frequency, our simple approach is sufficient for the data in hand.

Scattering times are only reported for bursts that satisfy two main criteria: 1) A combination of sufficient S/N and burst bandwidth – in practice, a S/N $\gtrsim 5$ in at least 2 frequency subbands, where a given subband is typically > 20 MHz wide; and 2) there is a global minimum in χ^2 and τ has a fractional error $< 30\%$. We refer to bursts that fit these criteria as Set 1. Bursts that do not meet these criteria are called Set 2. Set 2 contains both low S/N bursts that do not meet criterion (1), and high S/N bursts that do not meet criterion (2).

2.4 The Skewness Test

To constrain the presence of scattering for bursts in Set 2, we develop a two-part metric based on the skewness function (Stinebring & Cordes 1981). The skewness function quantifies the degree and direction of asymmetry in a burst of intensity $I(t)$, and is given by

$$\kappa(\delta t) = \frac{\langle I^2(t)I(t + \delta t) \rangle - \langle I(t)I^2(t + \delta t) \rangle}{\langle I(t) \rangle^3}, \quad (1)$$

where brackets denote time averages and δt is a given time lag. Typically the skewness function is normalized using the third moment $\langle I^3(t) \rangle$, but this normalization yields a strong S/N dependence that renders large errors for many bursts in our sample. We mitigate this effect by normalizing with the mean $\langle I(t) \rangle^3$. For an asymmetric pulse, the skewness function is antisymmetric in δt , and maximizes at an amplitude κ_{max} and a lag δt_{max} . When calculating κ_{max} and

δt_{\max} we only consider lags less than twice the burst width inferred from the ACF.

The two-part skewness test assesses both the sign of δt_{\max} and the amplitude κ_{\max} . For an exponential PBF, $\kappa(\delta t)$ maximizes at $\delta t_{\max} = \tau \ln 2$, and κ_{\max} increases with respect to τ . For a Gaussian pulse convolved with an exponential PBF, $\delta t_{\max}/\ln 2 > \tau$. Noise can induce both positive and negative temporal asymmetries. For high S/N bursts this effect is negligible and the sign of δt_{\max} for an individual burst provides one piece of evidence for scattering. A sample of noisy, intrinsically symmetric bursts will have equal probability of δt_{\max} being positive or negative, but a sample of noisy, scattered bursts will preferentially have $\delta t_{\max} > 0$. One could also argue that intrinsically asymmetric bursts will not preferentially be biased towards positive temporal asymmetries. The distribution of δt_{\max} for a sample of independent bursts is thus also used to assess the presence of scattering.

The second part of the skewness test assesses the amplitude κ_{\max} . When the S/N of a given burst is high (the exact S/N threshold depends on the burst width; see Appendix A), the amplitude of the maximum skewness κ_{\max} is compared to the maximum skewness of an exponential PBF with the same total width as the observed burst. The resulting ratio of skewness amplitudes is then compared to the ratio that would be obtained for a Gaussian burst, in order to determine whether the observed skewness is consistent or inconsistent with scattering to a given statistical confidence level. The full procedure for assessing the skewness amplitude κ_{\max} is described in Appendix A.

2.5 Mean Scattering Times from Fourier Domain Stacking

In O22 we demonstrated that stacking bursts' temporal profiles in the Fourier domain can be used to infer an average scattering time. This method has the advantage of mitigating shifts in burst arrival times both across the frequency band of a single burst and when stacking different bursts. Here we employ an identical routine to compare the average scattering times of bursts in Sets 1 and 2, as follows: burst temporal profiles were obtained by averaging each burst over two frequency subbands, 1.29-1.37 GHz, and 1.37-1.45 GHz. The power spectra (equivalent to the squared magnitude of the fast Fourier transform) of all burst profiles falling within a given subband were then stacked to compute an average power spectrum for each frequency subband. In O22, an additional frequency subband from 1.05-1.25 GHz was used, but the number of bursts falling within this subband is too small to compute an average power spectrum for this subband from Sets 1 and 2 separately. The average power spectrum was then fit with the canonical scattering model, where the spectrum consists of the product of Gaussian and PBF contributions. The error in τ inferred from this method includes contributions from the rms fluctuations of the individual power spectra about the mean spectrum, and from the rms residuals between the mean power spectrum and the fitted model. A complete description of the stacking method is provided in O22.

3 ANALYSIS & RESULTS

Bursts A-C in Figure 1 and Figure 2a show examples of bursts in Set 1, which have best-fit scattering times of 6.7 ± 0.4 ms, 6.2 ± 0.7 ms, and 7.9 ± 0.4 ms at 1.45 GHz for bursts A, B, and C, respectively. Set 1 also contains significant scattering measurements for thirteen other bursts (Table 1), which we compare to bursts in Set 2 below.

MJD	τ (ms at 1.45 GHz)	Gaussian FWHM (ms)	DM (pc cm ⁻³)
58991.68687	6.5 ± 0.9	5.9 ± 0.7	1210 ± 5
58991.70463	6.7 ± 1.4	5.7 ± 2.2	1210 ± 4
58991.71769	7.4 ± 0.3	7.5 ± 0.2	1219 ± 5
58991.71788	6.1 ± 1.5	5.7 ± 1.5	1222 ± 4
58991.71822	8.5 ± 0.2	10.6 ± 0.2	1211 ± 7
59060.48447	7.9 ± 0.3	9.7 ± 0.5	1187 ± 11
59060.50785	6.9 ± 0.3	4.2 ± 0.5	1196 ± 13
59060.52596	7.0 ± 0.3	6.8 ± 0.4	1205 ± 10
59061.52434 ^A	6.7 ± 0.4	5.4 ± 0.4	1196 ± 9
59061.54182 ^B	6.2 ± 0.7	12.2 ± 1.2	1210 ± 5
59067.50989	6.9 ± 0.5	3.5 ± 0.5	1213 ± 5
59067.53524	5.9 ± 0.4	6.8 ± 0.5	1202 ± 9
59069.51499	7.6 ± 0.5	5.4 ± 0.2	1210 ± 7
59077.46629	6.9 ± 0.4	7.1 ± 0.5	1190 ± 4
59077.46990	9.1 ± 0.7	4.5 ± 0.2	1180 ± 10
59077.47533 ^C	7.9 ± 0.4	8.9 ± 0.5	1217 ± 11
59077.47744 ^D	< 3.1	2.9 ± 0.1	1197 ± 3

Table 1. Scattering times for bursts in Set 1. Burst arrival times are quoted in modified Julian date (MJD) to a precision of about one second, and are referenced to the Solar System barycentre at 1.5 GHz. Scattering times τ were measured using a 2D fitting routine that assumes $\tau \propto \nu^{-4}$, and are referenced to 1.45 GHz by the same assumption. The fitting also assumes the Gaussian FWHM is constant across frequency. DMs shown maximize the S/N. Bursts A-D are indicated with superscripts.

Burst D (Figure 2b) stands out as having a much shorter scattering time than bursts in Set 1. It was detected only 2.9 minutes after burst C, with a scattering time that is at least a factor of two smaller. The ACF of the frequency-averaged burst profile yields an empirical measurement of the burst FWHM, $W = 2.9 \pm 0.1$ ms; the contribution of intra-channel dispersion smearing to the burst width is less than 1%. The burst peak signal-to-noise ratio S/N = 9.1 is too small to perform a least squares fit for scattering in both frequency and time. Figure 3 shows the results of fitting the 1D burst profile with a Gaussian pulse convolved with an exponential PBF, which yields $\tau(1.45 \text{ GHz}) = 1.5 \pm 0.4$ ms and a standard deviation $\sigma_G = 0.8 \pm 0.2$ ms with a reduced $\chi^2 = 1.2$. For the same Gaussian width, scattering times between 6 and 12 ms at 1.45 GHz (the approximate range of τ across the entire burst sample) would yield much larger temporal widths than observed from the burst profile. Fitting a symmetric Gaussian pulse to the burst yields $\sigma_G = 1.3 \pm 0.1$ ms with $\chi^2 = 1.4$, and hence is not preferred over the exponential model. As the peak S/N is too small to assess the frequency dependence of the burst width, we place a 95% confidence upper limit on the scattering time of $\tau < 3.1$ ms at 1.45 GHz, based on the empirical burst width measured from the ACF. The scattering reference frequency is (conservatively) taken to be the highest frequency at which the burst is detected. The DM of burst D (1197 ± 3 pc cm⁻³) is marginally different from that of burst C (DM = 1217 ± 11 pc cm⁻³). The τ upper limit for burst D is at least two times smaller than the scattering times measured for bursts A-C and the other bursts with individual scattering measurements, all of which are shown in Figure 4.

The scattering times shown for individual bursts in Figure 4 represent cases with both sufficient S/N and spectral bandwidth to perform a least squares fit that yields significant scattering measurements (these bursts constitute Set 1; see Section 2). From these bursts alone, one would infer that the mean scattering time is 6.9 ± 1.0 ms at 1.45 GHz, and that τ can fluctuate by at least a factor of two between bursts. However, bursts in Set 1 only constitute a fraction of the bursts observed. Set 2 contains 32 other bursts, five of which are

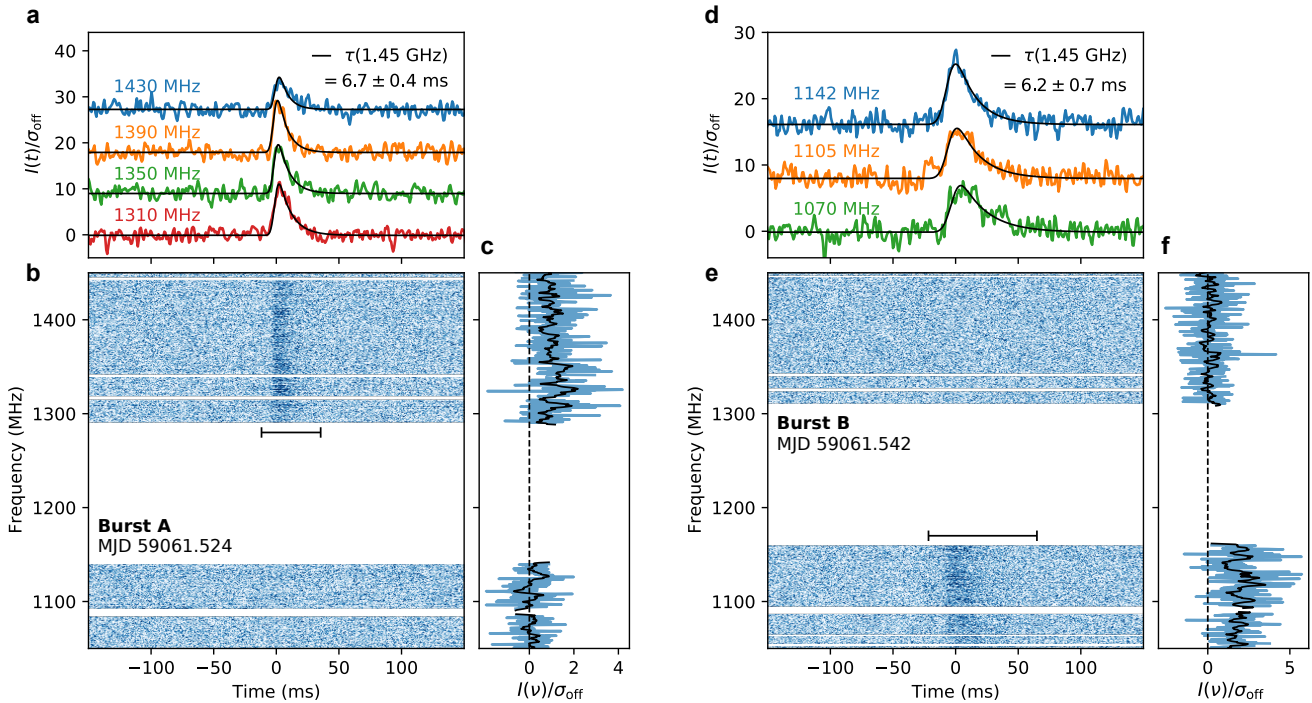


Figure 1. Two scattered bursts detected within 26 minutes. a) Frequency-averaged burst intensity vs. time in units of the signal $I(t)$ divided by the off-pulse noise σ_{off} and in four subbands centered on frequencies 1430 MHz (blue), 1390 MHz (orange), 1350 MHz (green), and 1310 MHz (red). Subbands are offset by an arbitrary amount for clarity. Black curves indicate the result of fitting a Gaussian pulse convolved with a one-sided exponential using a least squares fit for a Gaussian width fixed across frequency ν and a scattering time $\tau \propto \nu^{-4}$. The time resolution is 1.6 ms. b) Dynamic spectrum indicating burst intensity as a function of frequency vs. time. White bands are masked radio frequency interference (RFI). The horizontal black bar indicates the region used to calculate the time-averaged burst spectrum. c) Time-averaged burst spectrum vs. frequency ν in units of the signal-to-noise $I(\nu)/\sigma_{\text{off}}$ (blue curve) and the spectrum smoothed with a 1 MHz-wide boxcar filter (black curve). d) - f) Same as a) - c) for a burst detected below 1200 MHz. The scattering time was fit using the same procedure applied to the three frequency subbands shown in panel d): 1075 MHz (green), 1125 MHz (orange), and 1150 MHz (blue).

high S/N bursts that do not show the frequency dependence assumed in the canonical scattering model, either because they are inconsistent with any frequency-dependent temporal broadening or because their temporal widths decrease at lower observing frequencies. The rest of the Set 2 bursts have too low S/N to evaluate the scattering model on an individual burst basis.

In O22, we used Fourier domain stacking of bursts' temporal profiles (Section 2) to determine a mean scattering time $\bar{\tau}(1.45 \text{ GHz}) = 9.5 \pm 1.3 \text{ ms}$ for the same burst sample analyzed here. This mean scattering time was obtained using both high and low S/N bursts for which scattering can and cannot be measured individually, and is larger than most of the scattering times shown for Set 1 in Figure 4. This difference is partially due to a trade-off between intrinsic width and scattering: In general, τ can only be fit using the canonical scattering model when τ is greater than the intrinsic width in at least part of the frequency band. Figure 5 shows the distribution of total widths measured for bursts in Sets 1 and 2. Set 2 does contain more bursts with larger widths than Set 1, but a two-sided Kolmogorov-Smirnov test between the widths of Sets 1 and 2 bursts yields a p-value = 0.4, indicating that the total widths of the two burst sets are statistically consistent with being drawn from the same distribution. We also find no evidence of a strong correlation between burst total width and S/N in either burst set.

In order to assess whether the burst widths in Set 2 do include contributions from scattering, rather than simply having larger intrinsic widths, we examine both the skewness functions of the bursts and

re-perform the stacking analysis on Sets 1 and 2 separately.

Using the skewness test, we find that two bursts in Set 2 have skewness functions with significant evidence of scattering, based on both their skewness amplitudes and sign of $\delta t(\kappa_{\text{max}})$ (Section 2, Appendix A). The skewness test was inconclusive for most of the bursts in Set 2 because their S/N is too low to assess whether their maximum skewness amplitudes are consistent or inconsistent with scattering. Nonetheless, there are $8\times$ more bursts with positive δt_{max} than negative δt_{max} in Set 2, demonstrating that the sample of bursts in Set 2 is largely dominated by positive-handed temporal asymmetries. The distribution of δt_{max} for Set 2 is thus inconsistent with a population of intrinsically symmetric bursts with asymmetries contributed by noise alone. (For reference, all bursts in Set 1 have $\delta t_{\text{max}} > 0$.) We therefore conclude that bursts in Set 2 are overwhelmingly asymmetric and skewed to positive lags. While we have excluded bursts with identifiable sad-trombone drift from Set 2, we note that even unresolved drifting or an imprecise DM would not necessarily cause bursts to be preferentially skewed to positive lags.

The skewness test indicates that scattering is likely present in Set 2 bursts. We therefore apply the same Fourier domain stacking analysis used in O22 to Sets 1 and 2 separately, in order to determine whether the scattering in Set 2 is significantly different from that in Set 1. The mean and standard deviation of τ inferred from this analysis is shown in Figure 4 for both Sets 1 and 2. For Set 1, the stacking analysis yields $\bar{\tau}(1.45 \text{ GHz}) = 8.0 \pm 0.7 \text{ ms}$, whereas for Set 2, the stacking analysis yields $\bar{\tau}(1.45 \text{ GHz}) = 11.3 \pm 0.9 \text{ ms}$. The mean of these

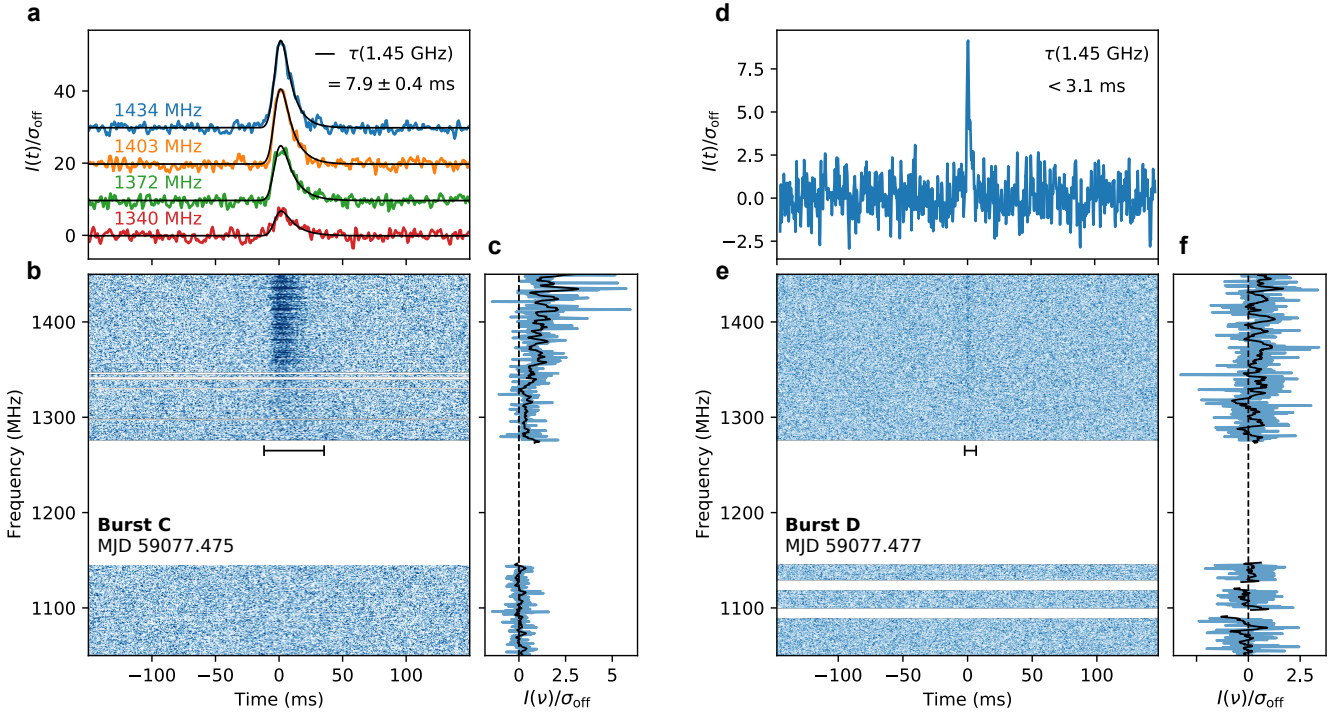


Figure 2. Two consecutive bursts with and without evidence of scattering. a) - c) Same as in Figure 1 for a burst detected at MJD 59077.475, with a scattering time $\tau = 7.9 \pm 0.4$ ms at 1.45 GHz. d) - f) Same as a) - c) for a burst detected at MJD 59077.477. In this case, the peak S/N is too low to divide the burst into multiple frequency subbands and test for frequency-dependent scattering. The burst full-width-at-half-maximum implies a 95% confidence upper limit on the scattering time $\tau < 3.1$ ms at 1.45 GHz.

values is consistent with the result presented in O22, which found $\bar{\tau}(1.45 \text{ GHz}) = 9.5 \pm 1.3$ using both Sets 1 and 2. Simply comparing the mean scattering times for Sets 1 and 2 confirms that τ varies by at least 40% across the burst sample, but comparing the scattering times of individual bursts in Set 1 to the mean scattering time of Set 2 suggests that τ may vary by up to 100% or more at 1.45 GHz.

While the difference in τ between bursts C and D suggests that τ can vary significantly over a timescale as rapid as 2.9 minutes, differences in τ are also seen between bursts detected on different days (Table 1). We have not found any significant evidence of correlations between the scattering times of Set 1 bursts, or any significant evidence of secular trends over time. We also find no obvious evidence for a correlation between τ and DM in Set 1. There are apparent DM fluctuations $\approx 5 - 10 \text{ pc cm}^{-3}$ between bursts, but these fluctuations are comparable to the measurement errors and may result from variations in burst structure. DM variations are expected at some level because variations in τ and RM are detected, and independent study of bursts detected at Green Bank Telescope and Parkes Telescope suggests that there are burst-to-burst variations in DM, albeit without a significant long-term (months to years-long) trend (Anna-Thomas et al. 2022). Future studies should continue to test for correlations in τ and DM between bursts, given that the sample of scattering times in Set 1 is sparse compared to the total number of bursts detected.

4 DISCUSSION

Independent observations of FRB 20190520B have associated the FRB with a persistent radio source (Niu et al. 2022) and RM vari-

ations over days to months have been detected from the FRB at frequencies above 2 GHz Anna-Thomas et al. (2022); Dai et al. (2022). Previous searches for RM in the same data set discussed in this work have yielded non-detections, with an upper limit of 20% on the degree of linear polarization (Feng et al. 2022; Niu et al. 2022). The degree of linear polarization increases substantially at higher frequencies (Feng et al. 2022; Anna-Thomas et al. 2022; Dai et al. 2022), suggesting that the non-detection of RM between 1.05 – 1.45 GHz is related to multi-path scattering that reduces the degree of linear polarization (Feng et al. 2022). However, there is no empirical evidence of a direct correlation between the scattering and RM variations, as these phenomena are observed at distinct radio frequencies.

All of these observations indicate a dynamic, multi-phase source environment. Scattering variations, in particular, imply fluctuations in weakly or non-relativistic, thermal ionized gas along the LOS. One physical model that can explain such fluctuations is a distribution of ionized cloudlets, or “patches,” that are slightly offset from the direct LOS. Scattering variations that are uncorrelated between bursts imply that each burst illuminates a small number of patches (perhaps only one). Patch sizes on the order of tens of au enclosed within a spherical volume of radius 1 pc can satisfy this requirement for bursts with emission durations of a few milliseconds (see Appendix B; a detailed paper on this patch model is in preparation). For bursts C and D, a significant change in τ over 2.9 minutes suggests that the length scale over which this change occurs is at most $c\Delta t \sim 0.4 \text{ au}$, where c is the speed of light. This scale is equivalent to an upper limit on the transverse offset between the two burst LOSs, which trace regions of significantly different scattering strength. This 0.4 au upper limit on the size scale is extremely conservative, given that

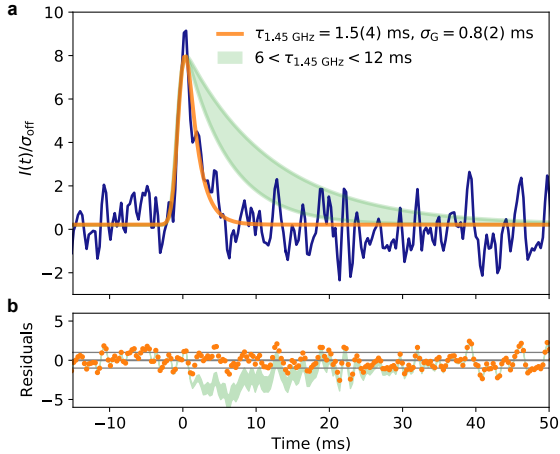


Figure 3. Comparison of the narrowest burst with average scattering. a) The dark blue curve shows the frequency-averaged burst intensity vs. time in signal-to-noise units $I(t)/\sigma_{\text{off}}$ for burst D, with a time resolution of 0.6 ms. The orange curve shows the result of fitting a Gaussian pulse convolved with an exponential PBF to the burst intensity, which yields a scattering time $\tau = 1.5 \pm 0.4$ ms and a Gaussian standard deviation $\sigma_G = 0.8 \pm 0.2$ ms. The reference frequency for τ is taken to be the highest frequency at which the burst is detected, 1.45 GHz. The filled green region demonstrates the range of scattering tails that would correspond to the same Gaussian width and the range of scattering times measured for other bursts in the sample, normalized to the same peak intensity as the orange model. b) Residuals between the measured burst intensity and the orange and green models shown in panel a). Residuals of ± 1 are indicated by the grey horizontal lines.

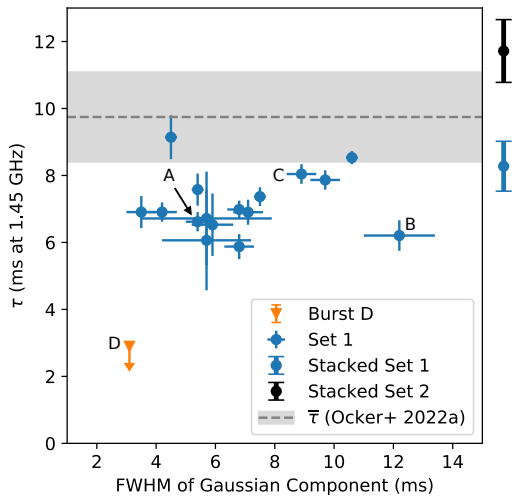


Figure 4. Burst scattering times and Gaussian widths. Blue points and errors correspond to the best-fit values and 68% confidence intervals for the scattering time τ in milliseconds at 1.45 GHz (top of the observing band) and the FWHM of the Gaussian burst component, fit using the same procedure as for bursts A-D. Sets 1 and 2 refer to bursts with and without significant least squares fits for τ and the Gaussian width, respectively. Also shown in orange is the upper limit on τ for burst D, the narrowest burst in the sample. The grey dashed line and shaded region correspond to the mean and standard deviation of τ inferred from stacking Sets 1 and 2 together in the Fourier domain (Ocker et al. 2022). The blue and black capped lines indicate the mean of τ and its standard deviation, inferred from applying the same stacking method to Sets 1 and 2, respectively (Methods).

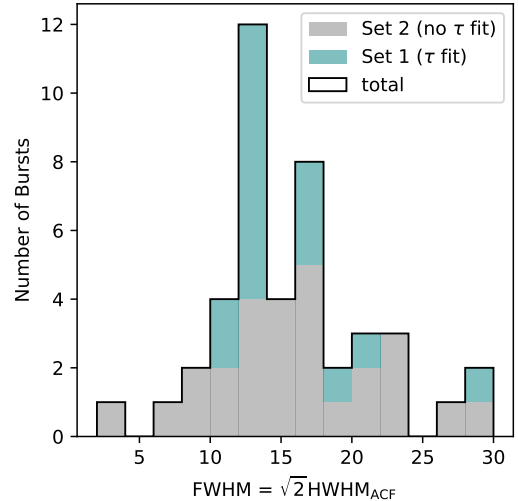


Figure 5. Distribution of total burst widths. The burst FWHM is defined as $\sqrt{2} \times \text{HWHM}$ of a burst's ACF, calculated from the burst profile integrated across the entire frequency band, 1.05 – 1.45 GHz (Methods). Full-widths for bursts in Set 1 (which have individual scattering measurements) are shown in green, and burst widths in Set 2 (no individual scattering measurements) are shown in grey. The average central frequency of the burst emission is 1350 MHz (Methods), and the total widths shown here are consistent with including the contributions of both scattering and intrinsic structure.

the actual size scale is probably related to the relative velocity of the source $v \ll c$ (where v is not known *a priori*). For typical pulsar velocities ~ 100 km/s (Verbunt et al. 2017) the size scale would be as small as thousands of kilometers.

Conservation of scattered burst flux occurs only for a very wide screen with homogeneous scattering properties. However, a patchy circumsource medium will cause dilution of burst flux in a manner that would likely correlate with scattering (Cordes & Lazio 2001). Patches could also be regions of significantly less scattering than the surrounding volume, and in this case the flux would be diluted except for LOS that pass through the patches. This effect may be difficult to identify in practice, given the large flux variability seen in FRBs for which scatter-broadening appears to be minimal (e.g. FRB 20121102A; Hessels et al. 2019; Li et al. 2021). For FRB 20190520B, we do not find significant evidence of a correlation between burst width and S/N, which would be one indicator of flux dilution from scattering (barring intrinsic flux variations, which are not accounted for). Refraction may also be relevant in the circumsource medium.

Analogous scattering variations have been observed from the Crab pulsar and are induced in its supernova remnant (Lyne & Thorne 1975; Backer et al. 2000; Lyne et al. 2001; McKee et al. 2018). Variations in the diffractive scattering time τ have been observed down to a resolution of 15 days over 30 years of archival data, and show a positive correlation with DM fluctuations $\lesssim 0.05$ pc cm $^{-3}$ (McKee et al. 2018). Refractive echoes have also been detected over months-long timescales (Backer et al. 2000; Lyne et al. 2001), and coincided with periods where the observed scattering deviated dramatically from the canonical scattering model (Backer et al. 2000; Lyne et al. 2001). Individual, giant pulses from the Crab also show evidence of multiple scattered trains (Sallmen et al. 1999). Changes in the scattering time could be correlated with orbital phase if the FRB source is in a binary system (which is one of the scenarios that could give rise to the large observed RM sign changes). Refraction

through a companion outflow could also periodically enhance the burst flux (Johnston et al. 1996; Main et al. 2018). All of these effects have been observed from Galactic pulsars (Johnston et al. 1996; Main et al. 2018; Andersen et al. 2022) and may be observable from FRB 20190520B, although we have not detected them in the data set considered here.

Regardless of the exact physical scenario, FRB local environments may not always yield burst structure consistent with the canonical scattering model typically assumed for burst shapes. Bursts' temporal structure can deviate from the canonical scattering model for several reasons: The exponential PBF applies to the special case of a Gaussian scattered image, but for non-Gaussian scattered images, the mean scattering delay will be greater than the $1/e$ time of an exponential PBF (Lambert & Rickett 1999). When the scattering screen is spatially well-confined (such as in a filament or discrete patch), the scattering strength is not uniform in directions transverse to the LOS, and the shape of the scattered image will be influenced by the physical extent of the screen rather than small (\ll au) scale plasma density fluctuations (Cordes & Lazio 2001). In this case, the frequency dependence of τ can be significantly shallower than ν^{-4} , and the scattering tail will be truncated (Cordes & Lazio 2001). We have identified two high S/N bursts from FRB 20190520B that do not show the frequency dependence expected from canonical scattering, but which have skewness functions with significant evidence of temporal asymmetries that may be related to scattering through a non-uniform screen (Appendix A). These effects, combined with the degree of variability we have characterized using the canonical scattering model, suggest that scattering may be variable in other FRBs, including as yet one-off FRBs that may not be representative of their source's local scattering medium, and repeating FRBs that have not yet shown obvious scattering. Scattering variations may be detectable regardless of whether sources also show RM variations and PRSs. Future searches for scattering variations from other repeating FRBs, in addition to correlations between scattering, flux, DM, and polarization, will illuminate how sub-parsec scale processes in FRBs' local environments shape burst propagation and observed spectra.

ACKNOWLEDGEMENTS

SKO, JMC, and SC acknowledge support from the National Science Foundation (AAG-1815242) and are members of the NANOGrav Physics Frontiers Center, which is supported by NSF award PHY-2020265. CHN is supported by the FAST Fellowship and DL acknowledges support from the National Natural Science Foundation of China (NSFC) Programs No. 11988101 and No. 11725313. JWM is a CITA Postdoctoral Fellow supported by the Natural Sciences and Engineering Research Council of Canada (NSERC), [funding reference #CITA 490888-16]. CJL acknowledges support from the National Science Foundation under Grant No. 2022546. RAT acknowledges support from NSF grant AAG-1714897.

DATA AVAILABILITY

The FAST data used in this paper are available at <https://doi.org/10.11922/sciencedb.o00069.00004>.

REFERENCES

Andersen B. C., et al., 2022, arXiv e-prints, p. arXiv:2209.06895

- Anna-Thomas R., et al., 2022, arXiv e-prints, p. arXiv:2202.11112
 Backer D. C., Wong T., Valanju J., 2000, *ApJ*, 543, 740
 Bij A., et al., 2021, *ApJ*, 920, 38
 Cordes J. M., Lazio T. J. W., 2001, *ApJ*, 549, 997
 Cordes J. M., McLaughlin M. A., 2003, *ApJ*, 596, 1142
 Dai S., et al., 2022, arXiv e-prints, p. arXiv:2203.08151
 Feng Y., et al., 2022, *Science*, 375, 1266
 Hessels J. W. T., et al., 2019, *ApJL*, 876, L23
 Johnston S., Manchester R. N., Lyne A. G., D'Amico N., Bailes M., Gaensler B. M., Nicastro L., 1996, *MNRAS*, 279, 1026
 Lambert H. C., Rickett B. J., 1999, *ApJ*, 517, 299
 Li D., et al., 2018, *IEEE Microwave Magazine*, 19, 112
 Li D., et al., 2021, *Nature*, 598, 267
 Lyne A. G., Thorne D. J., 1975, *MNRAS*, 172, 97
 Lyne A. G., Pritchard R. S., Graham-Smith F., 2001, *MNRAS*, 321, 67
 Main R., et al., 2018, *Nature*, 557, 522
 McKee J. W., Lyne A. G., Stappers B. W., Bassa C. G., Jordan C. A., 2018, *MNRAS*, 479, 4216
 Nan R., et al., 2011, *International Journal of Modern Physics D*, 20, 989
 Niu C. H., et al., 2022, *Nature*, 606, 873
 Ocker S. K., et al., 2022, *ApJ*, 931, 87
 Ruderman M. A., Sutherland P. G., 1975, *ApJ*, 196, 51
 Sallmen S., Backer D. C., Hankins T. H., Moffett D., Lundgren S., 1999, *ApJ*, 517, 460
 Stinebring D., Cordes J. M., 1981, *ApJ*, 249, 704
 Verbunt F., Igoshev A., Cator E., 2017, *A&A*, 608, A57

APPENDIX A: INTERPRETING THE SKEWNESS AMPLITUDE

For noisy pulses with a range of unscattered and scattered widths, the amplitude of maximum skewness κ_{\max} does not have a simple, deterministic relationship with scattering time τ . We therefore assess whether κ_{\max} for a given burst shows evidence of scattering by comparing the observed $\kappa_{\max}^{\text{obs}}$ to the value κ_{\max} would have if the burst were maximally asymmetric; i.e., if the entire burst width were contributed by the PBF. The ratio of maximum skew, $\kappa_{\max}^{\text{PBF}}/\kappa_{\max}^{\text{obs}}$, is then compared to the ratio that would be obtained for a Gaussian burst with the same observed total width and S/N, $\kappa_{\max}^{\text{PBF}}/\kappa_{\max}^{\text{Gauss}}$. This comparison of ratios is equivalent to testing whether an observed burst is distinguishable from a Gaussian. Figure A1 shows that the maximum skew ratio $\kappa_{\max}^{\text{PBF}}/\kappa_{\max}^{\text{Gauss}}$ is a linear function of S/N. The mean and rms error in this skewness ratio is computed from 500 independent white noise realizations. At high S/N, $\kappa_{\max}^{\text{PBF}} \gg \kappa_{\max}^{\text{Gauss}}$, because the Gaussian pulse's skewness is small compared to the skewness of a PBF with the same total width. At low S/N, noise dominates the skewness function, and the ratio $\kappa_{\max}^{\text{PBF}}/\kappa_{\max}^{\text{Gauss}}$ approaches unity. In this regime, the skewness function of the noisy Gaussian is indistinguishable from the skewness of an equivalent-width PBF. The slope of $\kappa_{\max}^{\text{PBF}}/\kappa_{\max}^{\text{Gauss}}$ and the S/N at which it reaches unity depend on pulse width. Figure A1 shows the best-fit linear model for $\kappa_{\max}^{\text{PBF}}/\kappa_{\max}^{\text{Gauss}}$ vs. S/N, for a Gaussian standard deviation $\sigma_{\text{Gauss}} = 10$ ms. This linear model scales with Gaussian width as roughly $\sigma_{\text{Gauss}}^{5.4}$.

In practice, we calculate the ratio of maximum skewness for each observed burst $\kappa_{\max}^{\text{PBF}}/\kappa_{\max}^{\text{obs}}$, assuming an exponential PBF of the total width inferred from the burst ACF. This ratio is then compared to the simulated mean and rms error of $\kappa_{\max}^{\text{PBF}}/\kappa_{\max}^{\text{Gauss}}$ for the same S/N and total width. If $\kappa_{\max}^{\text{PBF}}/\kappa_{\max}^{\text{Gauss}} \leq 1$ to within 95% confidence (based on the simulated error), the burst skewness falls in the noise-dominated regime, and the presence of scattering is considered indeterminate. If, on the other hand, $\kappa_{\max}^{\text{PBF}}/\kappa_{\max}^{\text{Gauss}} > 1$ (to at least 95% confidence), then the burst does not fall in the noise-dominated regime. In this case, a value of $\kappa_{\max}^{\text{PBF}}/\kappa_{\max}^{\text{obs}}$ consistent with $\kappa_{\max}^{\text{PBF}}/\kappa_{\max}^{\text{Gauss}}$ indicates that

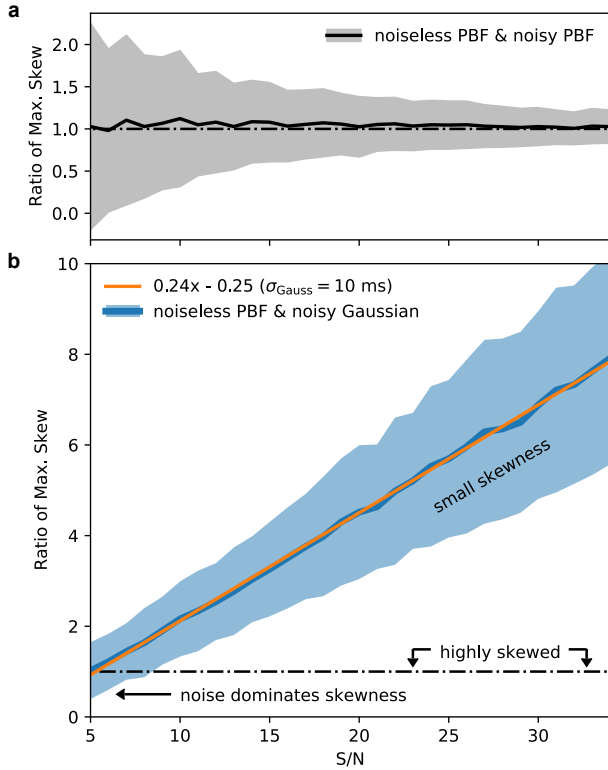


Figure A1. Simulated examples of the maximum skewness ratio for one-sided exponential and Gaussian pulses. a) Ratio of maximum skewness for a noiseless one-sided exponential PBF to a noisy PBF, as a function of S/N. The solid black line and shaded grey region correspond to the mean and standard deviation of the maximum skewness ratio for 500 independent noise realizations. The dashed-dotted black line indicates where the ratio equals one. b) The solid blue line and shaded region show the mean and standard deviation, respectively, of the maximum skewness ratio for a noiseless exponential PBF to a noisy Gaussian with a standard deviation $\sigma_{\text{Gauss}} = 10$ ms. The solid orange line indicates the best-fit linear model, which scales with Gaussian standard deviation as $\sigma_{\text{Gauss}}^{5.4}$. The dashed-dotted line indicates where the skewness ratio equals one. At high S/N values, the blue region corresponds to pulses with very small skewness, whereas high S/N pulses that have skewness ratios close to one are highly skewed. At low S/N values, noise dominates the skewness, and the maximum skewness of a noisy Gaussian pulse becomes indistinguishable from the maximum skewness of the PBF.

the burst skewness is smaller than expected from scattering, whereas a value of $\kappa_{\text{max}}^{\text{PBF}}/\kappa_{\text{max}}^{\text{obs}}$ less than $\kappa_{\text{max}}^{\text{PBF}}/\kappa_{\text{max}}^{\text{Gauss}}$ indicates that the burst skewness is consistent with scattering (at a given confidence interval based on the simulated error). Figures A2- A4 show comparisons between the observed skewness and skewness of an equivalent-width PBF for a burst in Set 1 and four bursts in Set 2, which demonstrate cases where the observed skewness is both consistent and inconsistent with scattering. The two bursts shown in Figure A4 are cases where a fit for the canonical scattering model was indeterminate, but both δt_{max} and κ_{max} reveal significant temporal asymmetries.

APPENDIX B: SCATTERING FROM DISCRETE PATCHES

Here we give an example of a physical model that explains scattering variations in terms of discrete patches distributed near the source.

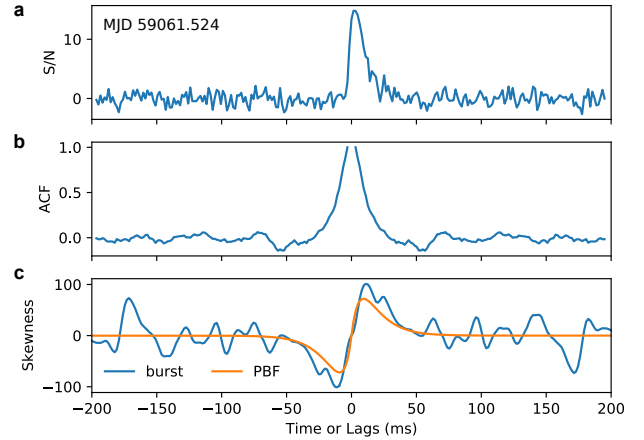


Figure A2. Intensity, autocorrelation, and skewness functions for a scattered burst. a) Frequency-averaged burst intensity vs. time in S/N units, for Burst A shown in Figure 1. This burst has a measured scattering time $\tau = 6.7 \pm 0.4$ ms at 1.45 GHz. b) Autocorrelation function (ACF) vs. time lag, calculated from the burst profile shown in panel (a). c) Skewness as a function of time lag for the measured burst profile (blue) and the skewness of a one-sided exponential pulse broadening function (PBF) with the same total width as the observed burst (orange). The total width was measured using the ACF. The ratio of the observed maximum skewness to the maximum skewness of the PBF is consistent with a very positively skewed burst, as expected from scattering.

This framework can be extended to a range of physical scenarios in which the circumsource medium is non-uniform.

Consider a rotating emission beam whose luminosity is highly intermittent. The burst emission has a duration Δt_e and a beam width $\Delta \theta_b$. The spin period of the beam is P_s . The emission beam rotates across a region of depth L , containing scattering patches of radius r_c and total transverse size $\Delta x \equiv 2r_c$ at typical separations Δl . A scattering patch is located at a distance d_{s1} from the source, and a distance d_{l0} from the observer. The source-to-observer distance d_{s0} and lens-to-observer distance d_{l0} are both much larger than d_{s1} .

In this model, a single burst would encounter a small number of patches. For simplicity, we assume here just one patch is illuminated. The number density of patches is $n_l \sim (\Delta l)^{-3}$. The mean free path for encountering a patch is $l_{\text{mfp}} = 1/(\pi n_l r_c^2)$. In order for a burst to encounter a single patch, $l_{\text{mfp}} \lesssim L$, implying an upper limit on the patch number density $n_l \lesssim 1/(\pi r_c^2 L)$. The total number of patches in a spherical volume surrounding the source is then $N_l \lesssim (4/3)(L/r_c)^2$.

There are two main constraints on the beam size $\Delta \theta_b$: It must be large enough to fully illuminate a patch, implying $\Delta \theta_b d_{s1} \sim \Delta \theta_b L \gtrsim \Delta x$, and it must be small enough that only one patch is illuminated, implying $\Delta \theta_b n_l L^3/3 \sim 1$. Assuming that Δl is some multiple m_l of the patch size, we then have $\Delta x/L \lesssim \Delta \theta_b \lesssim (3/L^2 n_l) \sim 3(m_l \Delta x/L)^3$, and $\Delta x/L \gtrsim \sqrt{1/3 m_l^3}$. The beam size is thus

$$\Delta \theta_b \lesssim (1/3 m_l^3)^{1/2} \approx 6 \times 10^{-4} (m_l/100)^{-3/2} \quad (\text{B1})$$

With relativistic beaming at a Lorentz factor γ , $\Delta \theta_b \gtrsim 1/\gamma$, implying $\gamma \lesssim 1700(m_l/100)^{3/2}$. A larger separation between patches increases the upper bound on the Lorentz factor. Lorentz factors $\sim 10^3 - 10^5$ have been inferred for radio pulsars (Ruderman & Sutherland 1975), including $\sim 10^4$ for Crab giant pulses (Bij et al. 2021), which provides one possible metric for comparing the emis-

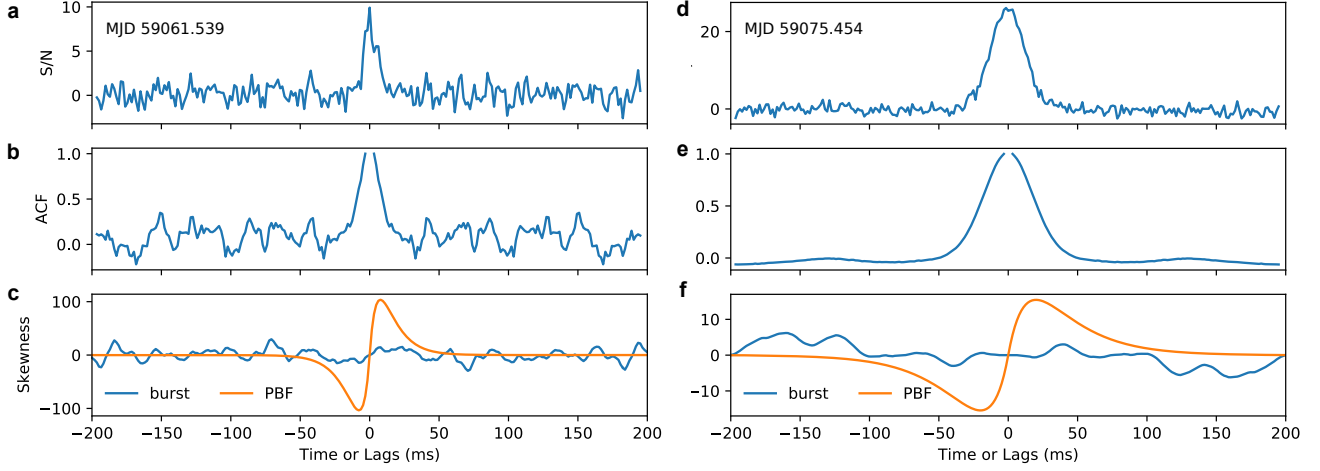


Figure A3. Intensity, autocorrelation, and skewness functions for two bursts without significant skewness. a) - c) Same as Figure A2a for a burst detected at MJD 59061.539. The ratio of the observed maximum skewness to the maximum skewness of the PBF is consistent with skewness dominated by noise, and the presence of scattering is indeterminate. d) - f) Same as a) - c) for a burst detected at MJD 59075.454. In this case, the S/N is high but the ratio of observed maximum skewness to the PBF maximum skewness is consistent with very small skewness, and the presence of scattering is again indeterminate.

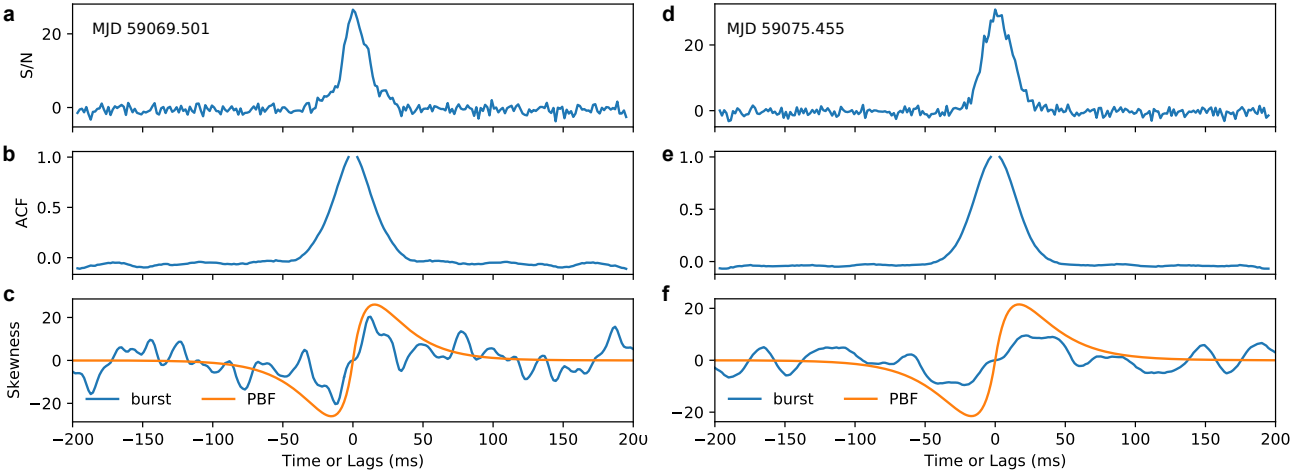


Figure A4. Intensity, autocorrelation, and skewness functions for two bursts with significant evidence of skewness. a) - c) Same as Figure A2a for a burst detected at MJD 59069.501. The ratio of the observed maximum skewness to the maximum skewness of the PBF is close to one, and is inconsistent with the ratio expected for a noisy Gaussian burst (see Figure A1) of the same width at 3σ confidence. d) - f) Same as a) - c) for a burst detected at MJD 59075.455. The ratio of the observed maximum skewness is again inconsistent with the ratio expected from a noisy Gaussian of the same width (2σ confidence). The canonical scattering model did not yield significant constraints on τ for either of these bursts.

sion mechanisms of FRBs and giant pulses.

The beam duration Δt_e must also be short enough that at most one patch is illuminated per spin period P_s . Assuming that the interval between bursts is much larger than P_s , we thus have $\Delta t_e \times (2\pi/P_s) \lesssim \Delta l/L$, or $\Delta t_e \lesssim \Delta l P_s / 2\pi L = m_l \Delta x P_s / 2\pi L$. For P_s in seconds the emission duration is then

$$\Delta t_e \lesssim 8 \text{ ms} \times \left(\frac{m_l}{100}\right) \left(\frac{\Delta x}{100 \text{ au}}\right) \left(\frac{P_s}{1 \text{ s}}\right) \left(\frac{1 \text{ pc}}{L}\right). \quad (\text{B2})$$

The narrowest burst we detect is 2.9 ± 0.1 ms wide, which points to either smaller m_l , Δx , or P_s , larger L , or some combination of the above. Nonetheless, emission durations on the order of milliseconds

are entirely consistent with patches \sim tens of au in transverse size distributed within a ~ 1 pc wide region around the source. Each patch contributes a DM $\sim 2n_e r_c \approx 4.8 \times 10^{-4} \text{ pc cm}^{-3} (r_c/50 \text{ au}) n_e$. Even for a density $\gg 1 \text{ cm}^{-3}$, this DM would be extremely small compared to the total DM of FRB 20190520B, which may explain why we do not detect any obvious temporal correlations between the observed scattering and DM.

This paper has been typeset from a $\text{\TeX}/\text{\LaTeX}$ file prepared by the author.